Human cytomegalovirus US21 protein is a viroporin that modulates calcium homeostasis and protects cells against apoptosis

Anna Luganini[a], Giovanna Di Nardo[a], Luca Munaron[a], Gianfranco Gilardi[a], Alessandra Fiorio Pla[a], and Giorgio Gribaudo[a,1]

[a]Department of Life Sciences and Systems Biology, University of Torino, 10123 Torino, Italy

Edited by Thomas E. Shenk, Princeton University, Princeton, NJ, and approved November 6, 2018 (received for review July 31, 2018)

The human cytomegalovirus (HCMV) US12 gene family comprises a set of 10 contiguous genes (US12 to US21) with emerging roles in the regulation of virus cell tropism, virion composition, and immunoevasion. Of all of the US12 gene products, pUS21 shows the highest level of identity with two cellular transmembrane BAX inhibitor motif-containing (TMBIM) proteins: Bax inhibitor-1 and Golgi anti-apoptotic protein, both of which are involved in the regulation of cellular Ca^{2+} homeostasis and adaptive cell responses to stress conditions. Here, we report the US21 protein to be a viral-encoded ion channel that regulates intracellular Ca^{2+} homeostasis and protects cells against apoptosis. Indeed, we show pUS21 to be a 7TMD protein expressed with late kinetics that accumulates in ER-derived vesicles. Deletion or inactivation of the US21 gene resulted in reduced HCMV growth, even in fibroblasts, due to reduced gene expression. Ratiometric fluorescence imaging assays revealed that expression of pUS21 reduces the Ca^{2+} content of intracellular ER stores. An increase in cell resistance to intrinsic apoptosis was then observed as an important cytobiological consequence of the pUS21-mediated alteration of intracellular Ca^{2+} homeostasis. Moreover, a single point mutation in the putative pore of pUS21 impaired the reduction of ER Ca^{2+} concentration and attenuated the antiapoptotic activity of pUS21wt, supporting a functional link with its ability to manipulate Ca^{2+} homeostasis. Together, these results suggest pUS21 of HCMV constitutes a TMBIM-derived viroporin that may contribute to HCMV's overall strategy to counteract apoptosis in infected cells.

human cytomegalovirus | US12 gene family | US21 protein | Ca^{2+} homeostasis | viroporin

Human cytomegalovirus (HCMV) is a major opportunistic pathogen and poses a huge threat to individuals with inadequacies in innate and adaptive immune responses. Indeed, HCMV is known to be a cause of life-threatening diseases in transplant recipients and the leading virus associated with congenital infections (1, 2). HCMV is a master at manipulating the host's defenses to promote its persistence (1–3). Indeed, a large portion of its protein coding potential is devoted not only to the regulation of cell tropism, dissemination, and reactivation within the host but also to the mitigation of immune responses (4). These genes are not strictly required for in vitro HCMV replication in fibroblasts and are therefore classified as nonessential (4). In fact, most of them are betaherpesvirus- or CMV-specific, clustered into families of related genes that may occur in tandem arrays or be dispersed within the HCMV genome (2, 4).

Among these nonessential HCMV genes is the US12 gene family, which includes a set of 10 contiguous tandemly arranged genes (US12 to US21) and constitutes about 5% of HCMV's genetic content (5). US12 family homologs have only been identified in CMVs specific to higher primates, such as rhesus CMV and chimpanzee CMV. The identification of putative seven-transmembrane hydrophobic domains in each of the US12 ORFs predicts a common structural framework that associates these proteins with cellular membranes (5). Moreover, amino acid sequence similarity, albeit at a low level, was observed between some US12 family ORFs and members of the Transmembrane Bax Inhibitor 1 Motif-containing (TMBIM) protein family, which modulate cellular Ca^{2+} homeostasis and adaptive responses to stress conditions (6, 7). However, despite the confirmed evolutionary importance of the US12 genes to HCMV biology (5), only a few functions have been associated with the family to date. US16, US18, and US20 have been implicated in determining HCMV cell tropism (8–10), US16 and US17 have been implicated in tuning virion composition (11, 12), and US12, US14, US18, and US20 have been implicated in evasion of natural killer cell activation (13–15).

Here, we report on the characterization of the late US21 protein as a viral-encoded Ca^{2+}-permeable channel able to reduce the Ca^{2+} content of intracellular stores. The pUS21-mediated alteration of Ca^{2+} homeostasis affects the susceptibility of cells to apoptosis, thus promoting cell survival and prolonging viral replication.

Results

Expression of US21 Protein. To characterize the expression of the US21 ORF, we generated a derivative of the low-passage

Significance

During coevolution with its host, human cytomegalovirus (HCMV) has invested a large part of its protein coding potential to ensure the dysregulation of the majority of cellular homeostatic circuits. Defining the role of these HCMV proteins is important to understand viral pathogenesis and to design new antiviral strategies able to exploit their functions. Here, we report on the functional characterization of the protein encoded by the US21 gene, the founding member of the HCMV US12 gene family. The pUS21 acts as a calcium-permeable multitransmembrane channel able to reduce the calcium content of intracellular stores; pUS21-mediated tampering with intracellular calcium homeostasis, in turn, decreases the cells' susceptibility to apoptosis, thus contributing to the overall HCMV protein toolbox evolved to blunt apoptosis in infected cells.

Author contributions: A.L. and G. Gribaudo designed research; A.L., G.D.N., and A.F.P. performed research; G.D.N. and A.F.P. contributed new reagents/analytic tools; A.L., G.D.N., L.M., G. Gilardi, A.F.P., and G. Gribaudo analyzed data; and A.L., G.D.N., A.F.P., and G. Gribaudo wrote the paper.

The authors declare no conflict of interest.

This article is a PNAS Direct Submission.

[1]To whom correspondence should be addressed. Email: giorgio.gribaudo@unito.it.

This article contains supporting information online at www.pnas.org/lookup/suppl/doi:10.1073/pnas.1813183115/-/DCSupplemental.

Published online December 10, 2018.

virus strain (TR) of HCMV, TRUS21HA, in which the HA epitope was fused at the C terminus of the US21 ORF (*SI Appendix*, Fig. S1). Expression of the tagged pUS21 was monitored by immunoblot analysis of whole-cell proteins prepared at different times postinfection (p.i.) from human foreskin fibroblasts (HFFs) infected with TRUS21HA. The pUS21, a protein of about 23.5 kDa, showed an expression pattern consistent with true late gene kinetics (Fig. 1*A*). The intracellular location of pUS21HA was investigated by confocal microscopy of HFFs infected with TRUS21HA. The pUS21HA was first detectable at 48 h p.i. with a diffuse pattern throughout the cytoplasm; then, from 72 h p.i., it accumulated in peripheral cytoplasmic structures (Fig. 1*B*). The staining pattern of pUS21HA almost completely overlapped with that of calreticulin (CALR), an endoplasmic reticulum (ER) marker (Fig. 1*B*, *Right*), but not with that of mitochondria (*SI Appendix*, Fig. S2), thus indicating that pUS21 associates with ER-derived vesicles over the entire HCMV replication cycle. Interestingly, pUS21HA did not show any significant colocalization with cellular and viral markers of the cytoplasmic virion assembly compartment (cVAC), such as GM130 (Fig. 1*B*, *Left*), EEA1, CD63, and gB (*SI Appendix*, Fig. S3) (16). The cVAC is a specialized compartment in HCMV-infected cells in which virions acquire their final tegumentation and envelope (16, 17), thus suggesting that pUS21, in contrast with other US12 family members, such as US16 and US17 (11, 12), is unlikely to be involved in the final maturation step of HCMV virions.

To investigate the membrane topology of pUS21, the potential transmembrane domain (TMD) regions of pUS21 were predicted using five different algorithms: Phyre, MEMSAT3,

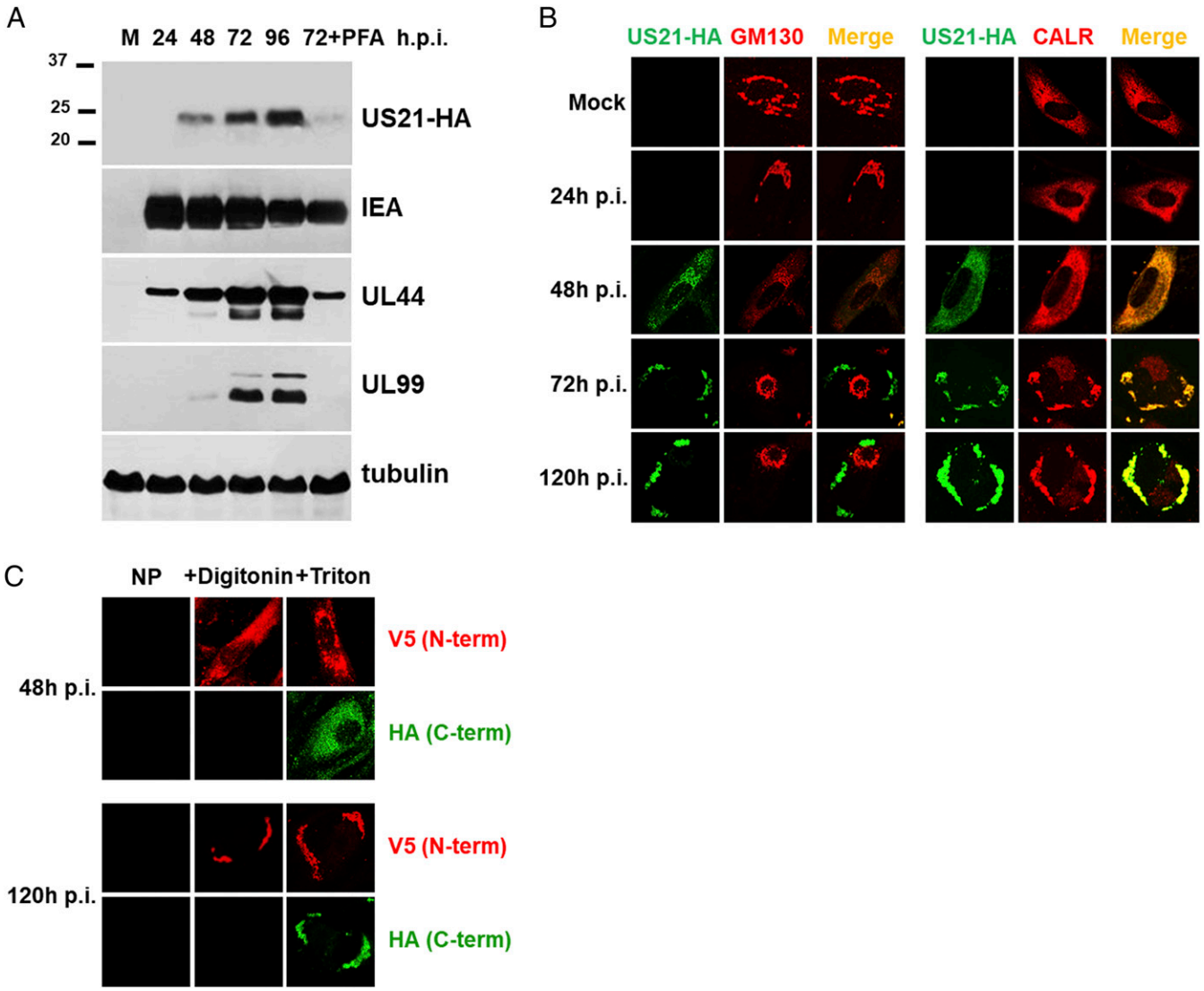

Fig. 1. Characterization of US21 protein expression. (*A*) Kinetics of pUS21 expression during HCMV infection. HFFs were infected with TRUS21HA [multiplicity of infection (MOI) of 1 pfu/cell]. At the indicated times p.i., protein cell extracts were analyzed by immunoblotting with anti-HA, IEA, UL44, UL99, or tubulin MAbs. The expression levels of IEA (IE1 and IE2), UL44, and UL99 were assessed as controls for representative IE, E, and L proteins, respectively. Cell extracts were from mock-infected cells (M); cells infected for 24, 48, 72, and 96 h; or cells infected and treated with phosphonoformic acid (PFA) (200 μg/mL) for 72 h. (*B*) Intracellular localization of pUS21HA during HCMV replication cycle. HFFs were infected with TRUS21HA (MOI of 1 pfu/cell) or mock infected, and, at various times p.i., cells were fixed, permeabilized, and immunostained with an anti-HA (green) and either (*Left*) GM130 (Golgi marker, red) or (*Right*) CALR (ER marker, red) MAbs. (*C*) Membrane topology of pUS21. HFFs were infected with TRUS21NV5-CHA (MOI of 1 pfu/cell), and, at 48 h or 120 h p.i., cells were not permeabilized (NP), or selectively or completely permeabilized using digitonin (+Digitonin) or Triton X-100 (+Triton). The pUS21 N- and C-terminal tags were then immunostained with MAbs to V5 and HA, respectively. Images in *B* and *C* are representative of three independent experiments. (Magnification in *B* and *C*: 60x.)

MEMSAT_SVM, TopPred, and TMHMM (18, 19). All algorithms were consistent in predicting seven TMDs with a cytoplasmic N terminus and a C terminus located on the luminal side of the membrane. To verify this prediction, the topology of pUS21 was assessed by selective permeabilization assay (20) of HFFs infected with another TR derivative, the TRUS21NV5-CHA (*SI Appendix*, Fig. S1). Selective permeabilization assay with digitonin or Triton X-100 was first validated using cellular (GM130 and CALR) and viral (gB, gH, and pp65) markers (*SI Appendix*, Fig. S4). Immunostaining of V5 and HA epitopes, following selective permeabilization of TRUS21NV5-CHA–infected cells, confirmed that the N terminus of pUS21 was located in the cytosol, while its C terminus was within the vesicle lumen (Fig. 1*C*). These results uphold the predicted seven-TMD topology of pUS21. Taken together, the results shown in this section indicate pUS21 to be a late HCMV protein with a seven-TMD architecture that localizes to ER-derived vesicles.

pUS21 Is Required for Efficient HCMV Replication. To determine the importance of the US21 gene in the context of HCMV replication in different cell types, we generated another two TR derivatives in which the US21 ORF was either deleted, as in TRΔUS21, or inactivated by the insertion of a stop codon near the N terminus, as in TRU21stop (*SI Appendix*, Fig. S1). Multistep growth curves of infected HFFs and endothelial cells (HMVECs) revealed the replication of TRΔUS21 and TRUS21stop to be more than 10^2-fold lower in HFFs and 10^4-fold lower in HMVECs compared with TRwt or the revertant TRUS21HA, thus indicating that the defective-growth phenotype of US21-deficient viruses was due to the specific inactivation of the gene (Fig. 2*A*). The impeded replication of US21-null viruses was due to alterations in the HCMV replication cycle that affect postentry phases, as suggested by the nuclear accumulation of pp65 delivered into HFFs by genetically negative US21 virions that was indistinguishable from that of TRwt or TRUS21HA, thus indicating the successful entry of TRΔUS21 and TRUS21stop viruses and the dissociation of pp65 from the capsids (*SI Appendix*, Fig. S5). However, despite adequate entry, the US21-null virus expressed lower levels of representative IE, E, and L genes compared with TRwt, as assessed by both qRT-PCR of IE1, UL44, UL99, and UL32 transcripts (Fig. 2*B*) and the immunoblotting of IE, UL44, and UL99 proteins (Fig. 2*C*). Specifically, the reduced viral gene expression became significant starting from 72 h p.i. (Fig. 2*B*), by which time pUS21 was fully expressed (Fig. 1*A*). These results indicate that the lack of functional pUS21 in producer cells generated viruses with defects in postentry phases that affect viral growth in different cell types, thus suggesting the requirement of pUS21 for efficient HCMV replication.

The US21 Protein Is a Putative Ion Channel Regulating Ca^{2+} Homeostasis. The pUS21 shows the highest level of identity with Bax inhibitor-1 (BI-1) (19%) and Golgi anti-apoptotic protein (GAAP) (21%), two multifunctional TMBIM proteins with acknowledged roles in modulating Ca^{2+} homeostasis, apoptosis, ER stress, ROS production, cell migration, and adhesion (6). Despite the absence of crystal structures for any of the TMBIM proteins, the recent availability of high-resolution structures of the bacterial BI-1 homolog, YetJ, a seven-TMD Ca^{2+}-leak channel from *Bacillus subtilis*, has provided structural insights into some of the TMBIM-mediated activities (5, 21). Sequence alignments of pUS21 with BsYetJ, BI-1, human GAAP, and CMLV GAAP (the camelpox virus GAAP homolog) (Fig. 3*A*) revealed that the two TMBIM family conserved C-terminal aspartic acid residues (Asp171 on TMD6 and Asp195 on TMD7 in BsYetJ), needed for the regulation of Ca^{2+} channel activity of BsYetJ (21), aligned with Asp178 and Asp201 of pUS21, respectively (Fig. 3*A* and *SI Appendix*, Fig. S6). Based on the multiple conformation states defined by the crystal structures of BsYetJ (21), we then generated structural models of pUS21 in closed (Fig. 3*B*, *Left*) and open (Fig. 3*B*, *Middle*) conformations using the fold recognition approach. In the closed state, Asp178 on TMD6 and Asp201 on TMD7 were predicted to lie within the putative pUS21 pore and

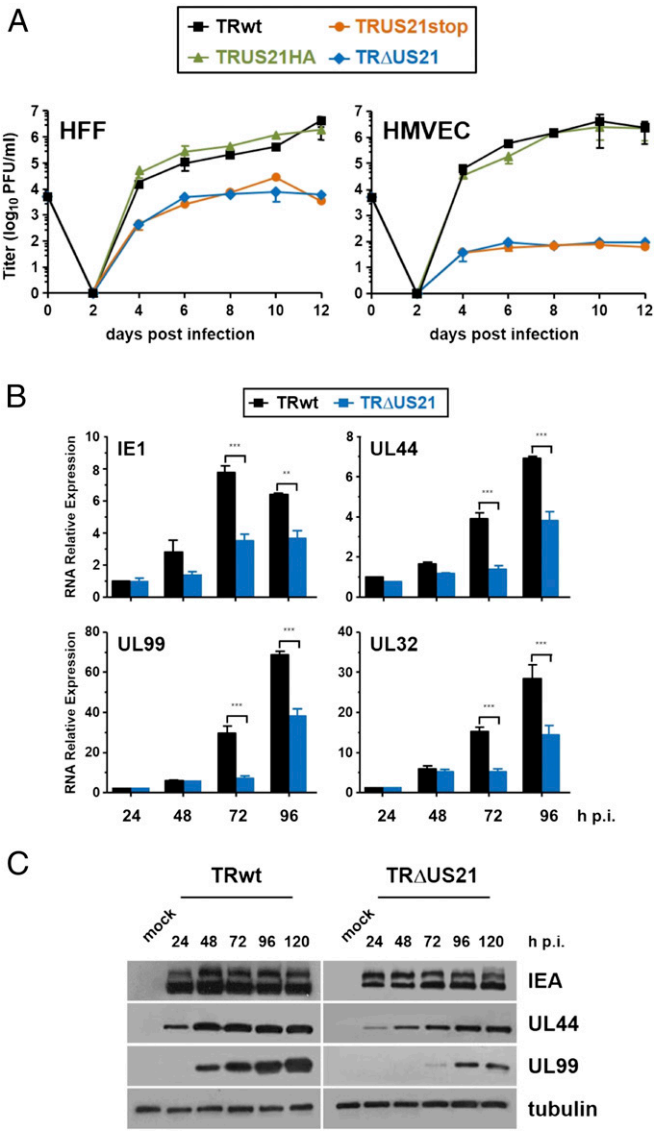

Fig. 2. Inactivation of US21 reduces HCMV replication. (*A*) Growth kinetics of US21-deficient viruses in fibroblasts and endothelial cells. HFFs and HMVECs were infected with TRwt, TRΔUS21, TRUS21stop, or TRUS21HA (MOI of 0.1 pfu/cell). The extent of virus replication at different times p.i. was then determined by plaque assay in HFFs. Data shown are the averages of three experiments ±SD. (*B*) The US21 gene is required for efficient viral gene expression. HFFs were infected with TRwt or TRΔUS21 (MOI of 1 pfu/cell), and total RNA was isolated at the indicated hours p.i. and reverse-transcribed. The qRT-PCR was carried out with the appropriate IE1, UL44, UL99, UL32, and β-actin primers. In the quantitative analysis, the values at each time point are relative to the value observed with cells infected with TRwt for 24 h (calibrator sample), which was set at 1. The results are the mean values of two independent experiments ± SD of technical triplicates. $^{**}P < 0.001$, $^{***}P < 0.0001$, versus calibrator sample. (*C*) Reduced levels of representative IE, E, and L proteins in cells infected with a US21-null virus. HFFs were infected with TRwt or TRΔUS21 (MOI of 1 pfu/cell) and total protein extracts were obtained at the indicated hours p.i. and analyzed by immunoblotting with anti-IEA, anti-UL44, and anti-UL99 mAbs.

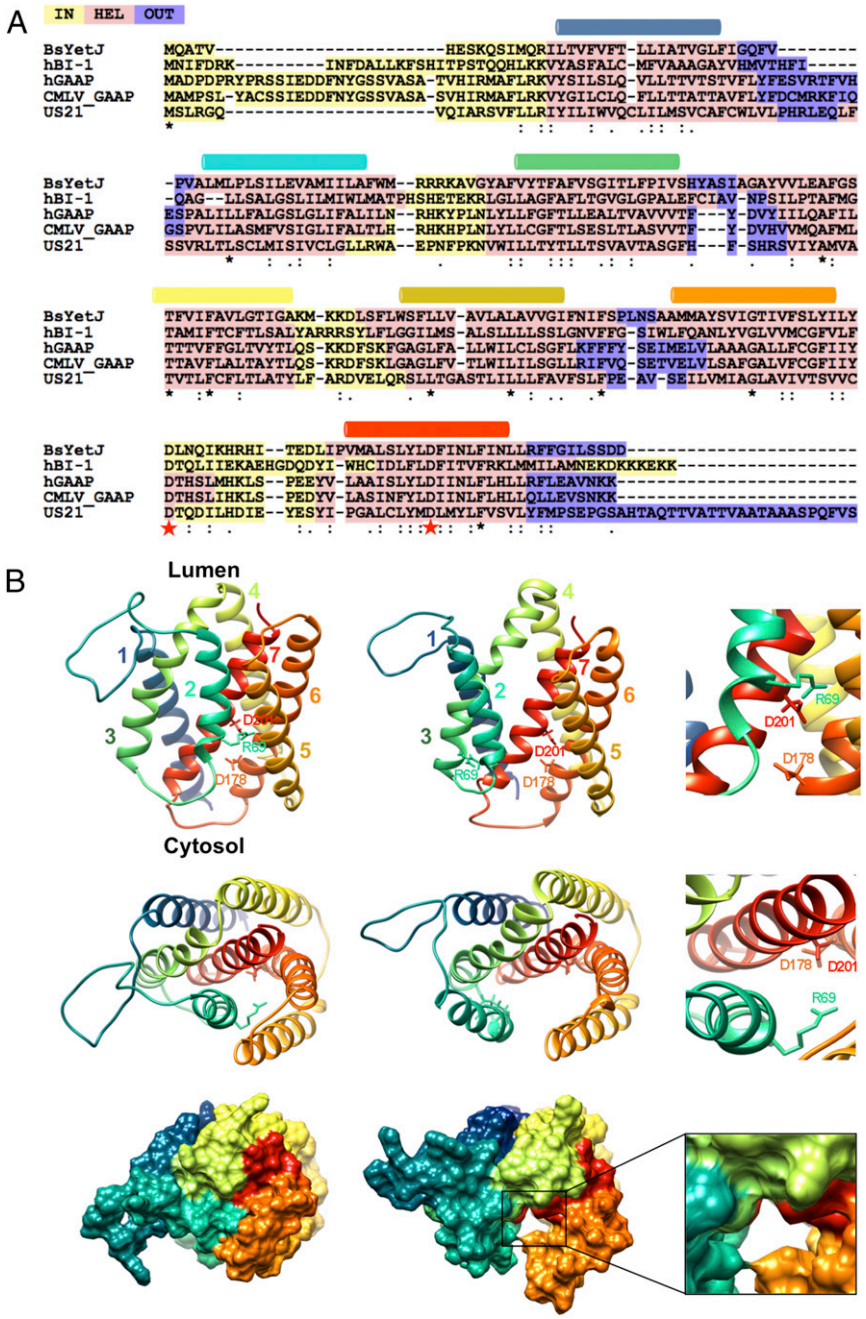

Fig. 3. Structural models of pUS21. (*A*) Amino acid alignments of pUS21 against bacterial BsYetJ and TMBIM family members. Multiple sequence alignment between pUS21, BsYetJ, hBI-1, hGAAP, and CMLV_GAAP was performed using TM-Coffee to highlight similarities, levels of identity, and differences between the proteins. Protein segments predicted to face the cytoplasmic ("IN") or luminal ("OUT") side of the membrane are highlighted in yellow and blue, respectively; those predicted to form part of the TMDs ("HEL") are shown in pink. The locations of the seven TMDs are indicated by colored bars: TMD1 (dark blue), TMD2 (light blue), TMD3 (green), TMD4 (light yellow), TMD5 (dark yellow), TMD6 (orange), and TMD7 (red). Red stars indicate the two conserved aspartate residues that form a diaspartyl sensor in BsYetJ. (*B*) Structural models of pUS21 are based on the crystal structures of BsYetJ. Models of pUS21 were generated using Phyre2 and are shown in the (*Left*) closed and (*Middle*) open conformations, and as viewed (*Upper*) from the membrane or (*Middle* and *Lower*) from the ER lumen. (*Right*) Enlarged regions of the closed state pUS21 model viewed from (*Upper Right*) the membrane and (*Middle Right*) the luminal side. (*Lower Right*) The boxed region of the open state model is also enlarged, showing the location of the predicted continuous protein pore across the membrane viewed from the luminal side. Arg69, Asp178, and Asp201 correspond to BsYetJ residues and are components of the putative channel-closing latch.

to interact with the positively charged Arg69 on TMD2 (Fig. 3*B*, *Right*), similarly to that observed in the closed structure of BsYetJ, in which Asp171 and Asp195 form hydrogen-bonded salt bridges between each other and with the basic Arg60 on TMD2 (5, 21). The disruption of these interactions by a decrease in pH via the protonation of Asp171 and Asp195 then leads to TMD2 conformational changes and the opening of the BsYetJ channel (5, 21). Similarly, in the predicted pUS21 open state, Asp178 and Asp201 are situated far from each other and even farther from Arg69 compared with their locations in the closed

state (Fig. 3*B*, *Right*), which may itself determine the disruption of their interactions and the opening of the pUS21 pore. Thus, in pUS21, Asp178 and Asp201 may form the TMBIM family conserved pH sensor able to regulate pUS21's putative Ca^{2+} channel activity via the detection of $[H^+]$ changes.

To verify this hypothesis experimentally, we investigated the effects of ectopic expression of pUS21 on intracellular Ca^{2+} homeostasis by means of Ca^{2+} imaging using the ratiometric fluorescent Ca^{2+} indicator Fura-2 AM (22). To this end, a tetracycline-regulated expression system was developed for efficient expression of HA-tagged pUS21 in cells that constitutively express the TR protein [the Tetracycline-Regulated Expression system (T-REx)-293]. This system that has been successfully used for the functional expression of Ca^{2+} channels (23) allows antibiotic-mediated expression of ion channel proteins without any adverse effect on host cells associated with their stable expression. The tetracycline-inducible expression of pUS21HA was confirmed by immunofluorescence (*SI Appendix*, Fig. S7) and immunoblotting (Fig. 4*A*, *Left*). Then, the ER Ca^{2+} content was indirectly evaluated in control or tetracycline-induced TREx-293-US21HA that had been loaded with Fura-2 AM. This probe is able to bind free Ca^{2+} in the cytoplasm, but not Ca^{2+} present in ER stores. In the presence of Ca^{2+}-free extracellular buffer (that prevents any Ca^{2+} influx from the extracellular environment), cell stimulation with ionomycin/thapsigargin induces Ca^{2+} release from intracellular stores. As shown in Fig. 4*A*, *Middle* and *Right*, in comparison with noninduced TREx-293-US21HA cells, the tetracycline-induced expression of pUS21HA significantly reduced the amount of releasable Ca^{2+} from intracellular stores as well as the basal Ca^{2+} content in the cytosol. Since pUS21 localized to ER-derived vesicles, we can assume that the observed decrease in the amount of Ca^{2+} content in intracellular stores following pUS21 expression (Fig. 4*A*) was consistent with passive leakage from the ER.

To investigate the importance of Asp178 and Asp201 for the Ca^{2+}-mobilizing activity of pUS21, the pUS21 mutants D178N and D201N were expressed as tetracycline-inducible proteins in TREx-293 cells (Fig. 4*B*, *Left*), and their ability to reduce the ER Ca^{2+} content was compared with that of pUS21HAwt (Fig. 4*B*, *Middle* and *Right*). Whereas pUS21HA-D178N did not behave differently from pUS21wt, mutation of D201 reversed the ability of pUS21wt to reduce the store's Ca^{2+} content, thus suggesting

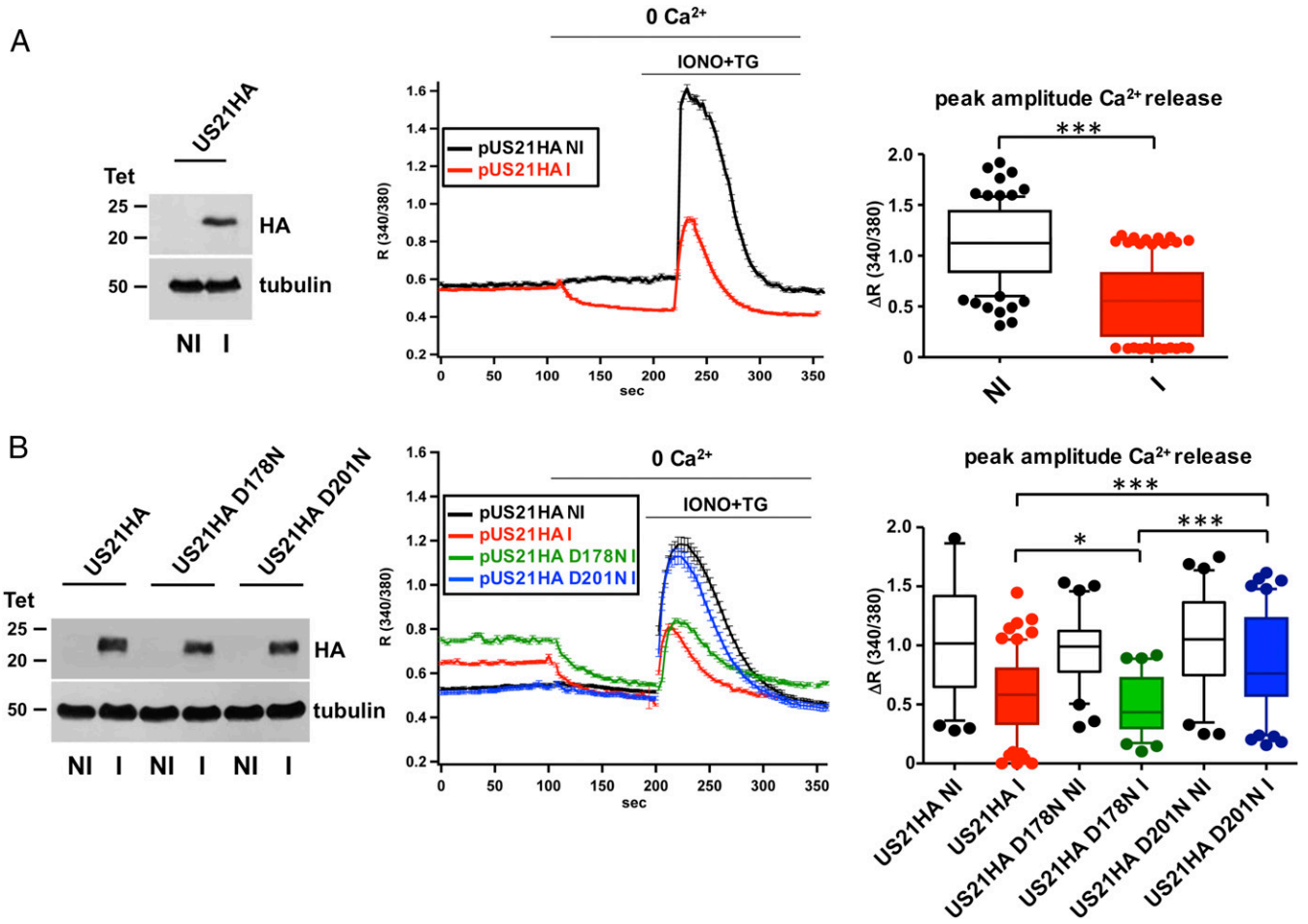

Fig. 4. The pUS21 forms a Ca^{2+}-permeable channel. (*A*) Expression of pUS21 reduces the agonist releasable Ca^{2+} content. (*Left*) Tetracycline-inducible expression of pUS21HA in TRex-293-US21HA cells was verified by immunoblotting. Protein extracts were from NI cells or I (1 μg/mL for 48 h) cells. (*Middle*) Time course of intracellular Ca^{2+} signals [R (340/380) in tetracycline-induced TRex-293-US21HA cells (red) compared with NI cells (black)]. Ca^{2+} signals were measured in ionomycin/thapsigargin-stimulated Fura-2 AM-loaded cells. (*Right*) Box and whisker plots show the maximum cytosolic Ca^{2+} concentrations ± SD of three experiments. ***$P <$ 0.0001, vs. TRex-293-US21HA cells NI. (*B*) Asp201 is important for pUS21 Ca^{2+} channel activity. (*Left*) Tetracycline-inducible expression of pUS21HA, pUS21HA-D178N, and pUS21HA-D201N in TRex-293-derived cell lines was verified by immunoblotting. Protein extracts were from NI cells or I cells. (*Middle*) Representative Ca^{2+} traces assessed in tetracycline-induced TRex-293-US21HA cells (red), TRex-293-US21HA-D178N cells (green), or TRex-293-US21HA-D201N cells (blue) compared with NI cells (black). Ca^{2+} signals were measured in ionomycin/thapsigargin-stimulated Fura-2 AM-loaded cells. Traces represent mean ± SD of three independent experiments. (*Right*) Box and whiskers plots show the maximum cytosolic Ca^{2+} concentrations ± SD of three experiments. ***$P < 0.0001$, *$P < 0.05$, vs. TRex-293-US21HA cells NI.

that Asp201 is located within the pore and is essential for the Ca^{2+} channel activity of pUS21.

Taken together, these results provide evidence that pUS21 forms a putative Ca^{2+}-conducting viroporin that determines a passive leaking of Ca^{2+} from ER, thus affecting intracellular Ca^{2+} homeostasis.

pUS21 Protects Cells Against Apoptosis. The mobilization of ER Ca^{2+} might have several consequences, including an impact on cell susceptibility to apoptosis (22, 24). To investigate whether the observed pUS21-mediated reduction of ER Ca^{2+} might correlate with a protective effect against proapoptotic signals, pUS21HAwt and the mutants D178N and D201N were transiently expressed in human embryonic lung fibroblast (HELF) cells (Fig. 5*A*) that were then challenged with staurosporine (STS), or doxorubicin (DOXO), as general triggers of the intrinsic apoptosis pathway. The activities of caspase-3 and caspase-7 were then measured as markers of apoptosis signaling cascades. Fig. 5 *B* and *C* shows that pUS21HA expression reduced caspase-3 and caspase-7 activation induced by either STS or DOXO. Among pUS21 mutants, only the D201N defective in reducing the Ca^{2+} content of ER stores attenuated the ability of pUS21wt to protect cells from apoptosis, thus indicating that this cytobiological consequence of pUS21 expression is related to its ability to manipulate intracellular Ca^{2+} homeostasis.

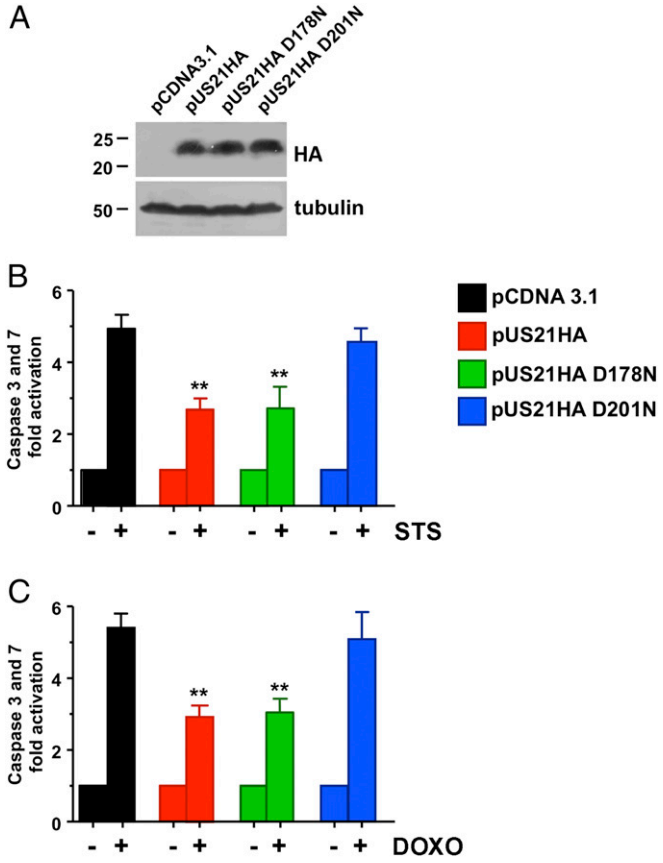

Fig. 5. The pUS21 expression decreases cell susceptibility to intrinsic apoptosis. HELF cells were transfected with pcDNA3.1, pUS21HA, pUS21HA-D178N, or pUS21HA-D201N. At 48 h posttransfection, expression of US21 proteins was confirmed by immunoblotting. (*A*) Transfected cells were either mock-treated or treated with STS (0.5 μM, 6 h), (*B*) or with DOXO (3 μM, 48 h), (*C*) before measuring caspase-3 and caspase-7 activities. Data shown are the averages of six independent experiments ± SD. $^{**}P < 0.001$ vs. pcDNA3.1+STS/DOXO.

Discussion

The observation of pUS21 as a remote TMBIM homolog (Fig. 3*A*), its conservation among US12 family members of different CMVs, and its location on a well-diverged branch separate from all other US12 proteins in phylogenetic analysis together support the view that US21 may represent the initial point of entry of the US12 gene family into an ancestral primate CMV (6). These facts suggest that the US21 gene of HCMV may actually be the descendant of a precursor TMBIM gene captured more than 40 Mya by an ancestral primate CMV (25). The low level of conservation between pUS21 and TMBIM proteins sustains the old timeframe of such an acquisition.

Nevertheless, due to functional requirements, some amino acid residues critical for the Ca^{2+}-conducting activity of TMBIM can still be found in pUS21. In fact, the most C-terminal Asp residue (D201) of the putative pUS21 diaspartyl sensor (D178 and D201) aligns with D213 of BI-1 and D219 of GAAP (Fig. 3*A*). The importance of BI-1 D213 and GAAP D219 for channel conductance has been demonstrated by the observation that their mutation attenuates the ability of BI-1 and GAAP to reduce the Ca^{2+} content of intracellular stores (26–28). Similarly, we observed that the mutation of D201 prevented the pUS21-mediated reduction of the Ca^{2+} content of the ER (Fig. 4*B*), thus suggesting that D201 lines the pUS21 pore and that it is indeed involved in its Ca^{2+} channel activity.

All human TMBIM proteins (TMBIM1-6) have been shown to reduce the Ca^{2+} content of intracellular stores (29), and their ability to modulate intracellular Ca^{2+} homeostasis is thought to be the core function through which they regulate different adaptive responses to stress conditions (30). The observation that the mutation of D219 in GAAP affects both channel conductance and the inhibition of apoptosis supports this hypothesis (28). Similarly, we observed that the mutation of D201 affects the ability of pUS21 to protect cells from apoptosis, suggesting that the modulation of Ca^{2+} plays a role in this pUS21-mediated cellular response.

Viroporins are viral ion channel proteins which dysregulate normal ionic homeostasis to promote viral replication and pathogenesis (22, 31). Based on the number and orientation of their TM segments, viroporins are classified as either class I (with a single TM) or class II (with two TMs). Recently, a third class of viral channels was proposed to accommodate viroporins containing six to seven TMs, such as the viral GAAP, which do not fit into either of the first two classes (30). Thus, pUS21 can be considered a Herpesvirus-encoded type III viroporin.

However, pUS21 is not the first HCMV protein to be described as acting as a viroporin. In fact, the protein product of UL37 exon 1 (UL37 × 1), termed vMIA (viral mitochondria-localized inhibitor of apoptosis), known to inhibit apoptosis by binding and sequestering Bax at the mitochondrial membrane (24, 32), was shown to localize to the ER and to induce Ca^{2+} release from ER stores (33). The vMIA-mediated dysregulation of Ca^{2+} homeostasis was related to the reorganization of the actin cytoskeleton, with the loss of F-actin and the accumulation of cortical actin, inducing cell rounding and swelling (33). This was then shown to occur through a Ca^{2+}-dependent protein kinase C pathway that also causes the accumulation of large lipid vesicles, a process important for virion morphogenesis (34).

The vMIA-mediated release of Ca^{2+} from ER was suggested to impact different adaptive cell responses to stresses, such as the unfolded protein response, modulation of mitochondrial functions, and protection against apoptotic stimuli (33). Accordingly, we observed that pUS21 expression reduced the activation of effector caspases upon STS stimulation, thus suggesting a protective role of pUS21 against apoptosis (Fig. 5). Given the crucial role of Ca^{2+} homeostasis in the apoptosis pathway, it is likely that modulation of the ER Ca^{2+} content by both vMIA and

pUS21 impacts the cell's susceptibility to apoptosis. In this scenario, the reduction in ER Ca^{2+} concentration caused by pUS21 or vMIA suggests that protection from apoptosis may derive from a reduced release of Ca^{2+} from ER stores in response to proapoptotic stimuli. This, in turn, would lead to a reduced entry of Ca^{2+} into mitochondria and thus decrease the extent of mitochondrial outer membrane permeabilization, the release of proaptogenic factors, and the activation of caspases (35).

Thus, pUS21 may contribute, together with vMIA, the viral inhibitor of caspase-8 activation (vICA), the protein product of the UL36 gene, and pUL38 (24, 32), to the overall antiapoptotic strategy of HCMV, thereby promoting the survival of infected cells even during the late phases of infection, to further sustain viral replication.

Materials and Methods

Bioinformatics and Protein Modeling. Sequence alignments were performed using TM-Coffee server. The GenBank (https://www.ncbi.nlm.nih.gov/Genbank) accession numbers for the proteins analyzed are the following: clinical isolate of HCMV TR Genome and US21 (AC146906.1); *H. sapiens* TMBIM6/BI-1 (NP_003208.2); *H. sapiens* TMBIM4/hGAAP (NP_001269535.1); CMLV TMBIM4/vGAAP (AAG37461.1); and *B. subtilis* YetJ (O31539). US21 topology was predicted using algorithms Phyre2, TopPred 0.01, MEMSAT3, MEMSAT_SVM, and TMHMM 2.0 (18, 19). The Phyre2 server was used for fold recognition-based modeling of pUS21. This analysis identified BsYetJ structures (21) as the templates for producing US21 models with the highest level of confidence (100%). The crystal structures of BsYetJ in the open [Protein Data Bank (PDB) ID code 4PGS] and closed (PDB ID code 4PGR) conformations were thus selected as templates to generate refined models of pUS21. The confidence scores for these pUS21 models in the open and closed conformations were −0.16 and −0.13 (PROCHECK G scores) and −1.08 and −2.01 (ProsA *z*-score), respectively—within the score ranges typically found for native proteins of a similar size, thus confirming their accuracy. Molecular graphics of the pUS21 models were generated using the UCSF Chimera package.

Cells and Viruses. HELFs, HFFs, and HMVECs were cultured as previously described (10, 11). T-REx-293 cells were grown in DMEM (Euroclone) supplemented with 10% FBS (Euroclone). Details on the generation of the TR-BAC (36) derivatives TRΔUS21, TRUS21stop, TRUS21HA, and TRUS21NV5-CHA (*SI Appendix*, Fig. S1) are provided in *SI Appendix*, *SI Materials and Methods*. Reconstitution of infectious HCMV, titration, and replication kinetics studies were all performed as described previously (10, 11).

US21 Protein Expression. Expression of pUS21HA was carried out using T-REx (Invitrogen). To this end, WT and mutated US21HA ORFs were cloned into pcDNA4/TO (Invitrogen) for tetracycline-inducible expression. The pUS21HA D178N and D201N mutations were generated using the Quickchange site-directed mutagenesis kit (Stratagene). For stable expression in TRex-293 cells, pcDNA4/TO-US212HA, pcDNA4/TO-US212HA-D178N, or pcDNA4/TO-US212HA-D201N were introduced using Lipofectamine 3000 (Invitrogen), and stable TRex-293 cell lines were selected using blasticidin and zeocin. To induce the expression of pUS21 in TRex-293–derived cell lines, tetracycline (1 μg/mL) was added for 48 h.

For transient expression in HELFs, cells were transfected with pcDNA3.1 (Invitrogen) and either pcDNA3.1-US21HA (pUS21HAwt), pcDNA3.1-US212HA-D178N (pUS21HA-D178N), or pcDNA3.1-US212HA-D201N (pUS21HA-D201N). At 48 h posttransfection, cells were either examined for the expression of US21 proteins by immunoblotting, mock-treated, or treated with STS (0.5 μM, 6 h) or with DOXO (3 μM, 48 h) before assessing caspase-3 and caspase-7 activities.

Analysis of RNA and Proteins. The qRT-PCR, immunoblotting, and immunofluorescence were carried out as described previously (10, 11). Additional details are provided in *SI Appendix*, *SI Materials and Methods*.

Apoptosis Assay and ATP Measurement. Levels of caspase-3 and caspase-7 activity were measured using the Caspase-Glo 3/7 substrate and the CellTiter-Glo assay (Promega). Luminescence was quantified using a Glomax luminometer (Promega).

Calcium Measurement. Ratiometric cytosolic Ca^{2+} ($[Ca^{2+}]i$) measurements were performed on noninduced (NI) or tetracycline-induced (I) TREx-293-US21HA cell lines that had been loaded (45 min at 37 °C) with 2 μM Fura-2 AM (Invitrogen) and imaged as previously described (37). Each fluorescent trace (340/380 nm ratio) represents a single region of interest corresponding to cells in the chosen image field. For the estimation of peak amplitude, only responses that had a $\Delta Em340/380 > 0.02$ were considered.

ACKNOWLEDGMENTS. We thank Jay Nelson for providing TR-BAC, Dong Yu for pGalK-Kan, and T. Shenk for pp71. We thank Noemi Cavaletto and Federica Galliano for their technical help. This work was supported by Ministero dell'Istruzione dell'Università e della Ricerca Projects of National Interest (Progetti di Ricerca di Interesse Nazionale) 2010-11 Grant 2010PHT9NF and a grant from Ricerca Locale.

1. Britt W (2008) Manifestations of human cytomegalovirus infection: Proposed mechanisms of acute and chronic disease. *Curr Top Microbiol Immunol* 325:417–470.
2. Mocarski ES, Shenk T, Griffiths PD, Pass RF (2013) Cytomegaloviruses. *Fields Virology*, eds Knipe DM, Howley PM (Lippincott, Philadelphia), 6th Ed, Vol 2, pp 1960–2014.
3. Luganini A, Terlizzi ME, Gribaudo G (2016) Bioactive molecules released from cells infected with the human cytomegalovirus. *Front Microbiol* 7:715.
4. Murphy E, Shenk T (2008) Human cytomegalovirus genome. *Curr Top Microbiol Immunol* 325:1–19.
5. Lesniewski M, Das S, Skomorovska-Prokvolit Y, Wang FZ, Pellett PE (2006) Primate cytomegalovirus US12 gene family: A distinct and diverse clade of seven-transmembrane proteins. *Virology* 354:286–298.
6. Liu Q (2017) TMBIM-mediated Ca^{2+} homeostasis and cell death. *Biochim Biophys Acta Mol Cell Res* 1864:850–857.
7. Rojas-Rivera D, Hetz C (2015) TMBIM protein family: Ancestral regulators of cell death. *Oncogene* 34:269–280.
8. Bronzini M, et al. (2012) The US16 gene of human cytomegalovirus is required for efficient viral infection of endothelial and epithelial cells. *J Virol* 86:6875–6888.
9. Hai R, et al. (2006) Infection of human cytomegalovirus in cultured human gingival tissue. *Virol J* 3:84.
10. Cavaletto N, Luganini A, Gribaudo G (2015) Inactivation of the human cytomegalovirus US20 gene hampers productive viral replication in endothelial cells. *J Virol* 89: 11092–11106.
11. Luganini A, Cavaletto N, Raimondo S, Geuna S, Gribaudo G (2017) Loss of the human cytomegalovirus US16 protein abrogates virus entry into endothelial and epithelial cells by reducing the virion content of the pentamer. *J Virol* 91:e00205–e00217.
12. Gurczynski SJ, Das S, Pellett PE (2014) Deletion of the human cytomegalovirus US17 gene increases the ratio of genomes per infectious unit and alters regulation of immune and endoplasmic reticulum stress response genes at early and late times after infection. *J Virol* 88:2168–2182.
13. Fielding CA, et al. (2014) Two novel human cytomegalovirus NK cell evasion functions target MICA for lysosomal degradation. *PLoS Pathog* 10:e1004058.
14. Fielding CA, et al. (2017) Control of immune ligands by members of a cytomegalovirus gene expansion suppresses natural killer cell activation. *eLife* 6:e22206.
15. Charpak-Amikam Y, et al. (2017) Human cytomegalovirus escapes immune recognition by NK cells through the downregulation of B7-H6 by the viral genes US18 and US20. *Sci Rep* 7:8661.
16. Das S, Pellett PE (2011) Spatial relationships between markers for secretory and endosomal machinery in human cytomegalovirus-infected cells versus those in uninfected cells. *J Virol* 85:5864–5879.
17. Tandon R, Mocarski ES (2012) Viral and host control of cytomegalovirus maturation. *Trends Microbiol* 20:392–401.
18. Kelley LA, Mezulis S, Yates CM, Wass MN, Sternberg MJE (2015) The Phyre2 web portal for protein modeling, prediction and analysis. *Nat Protoc* 10:845–858.
19. Nugent T, Jones DT (2009) Transmembrane protein topology prediction using support vector machines. *BMC Bioinformatics* 10:159.
20. Carrara G, Saraiva N, Gubser C, Johnson BF, Smith GL (2012) Six-transmembrane topology for Golgi anti-apoptotic protein (GAAP) and Bax inhibitor 1 (BI-1) provides model for the transmembrane Bax inhibitor-containing motif (TMBIM) family. *J Biol Chem* 287:15896–15905.
21. Chang Y, et al. (2014) Structural basis for a pH-sensitive calcium leak across membranes. *Science* 344:1131–1135.
22. Hyser JM, Estes MK (2015) Pathophysiological consequences of calcium-conducting viroporins. *Annu Rev Virol* 2:473–496.
23. O'Driscoll KE, Hatton WJ, Burkin HR, Leblanc N, Britton FC (2008) Expression, localization, and functional properties of Bestrophin 3 channel isolated from mouse heart. *Am J Physiol Cell Physiol* 295:C1610–C1624.
24. Galluzzi L, Brenner C, Morselli E, Touat Z, Kroemer G (2008) Viral control of mitochondrial apoptosis. *PLoS Pathog* 4:e1000018.
25. Davison AJ, et al. (2013) Comparative genomics of primate cytomegaloviruses. *Cytomegaloviruses: From Molecular Pathogenesis to Intervention*, ed Reddehase MJ (Caister Academic, Norwich, UK), Vol 1, pp 1–22.
26. Bultynck G, et al. (2012) The C terminus of Bax inhibitor-1 forms a Ca^{2+}-permeable channel pore. *J Biol Chem* 287:2544–2557.
27. Bultynck G, Kiviluoto S, Methner A (2014) Bax inhibitor-1 is likely a pH-sensitive calcium leak channel, not a H^+/Ca^{2+} exchanger. *Sci Signal* 7:pe22.

28. Carrara G, et al. (2015) Golgi anti-apoptotic proteins are highly conserved ion channels that affect apoptosis and cell migration. *J Biol Chem* 290: 11785–11801.
29. Lisak DA, et al. (2015) The transmembrane Bax inhibitor motif (TMBIM) containing protein family: Tissue expression, intracellular localization and effects on the ER CA^{2+} -filling state. *Biochim Biophys Acta* 1853:2104–2114.
30. Carrara G, Parsons M, Saraiva N, Smith GL (2017) Golgi anti-apoptotic protein: A tale of camels, calcium, channels and cancer. *Open Biol* 7:170045.
31. Zhou Y, Frey TK, Yang JJ (2009) Viral calciomics: Interplays between Ca2+ and virus. *Cell Calcium* 46:1–17.
32. Brune W, Andoniou CE (2017) Die another day: Inhibition of cell death pathways by cytomegalovirus. *Viruses* 9:E249.
33. Sharon-Friling R, Goodhouse J, Colberg-Poley AM, Shenk T (2006) Human cytomegalovirus pUL37x1 induces the release of endoplasmic reticulum calcium stores. *Proc Natl Acad Sci USA* 103:19117–19122.
34. Sharon-Friling R, Shenk T (2014) Human cytomegalovirus pUL37x1-induced calcium flux activates PKC**α**, inducing altered cell shape and accumulation of cytoplasmic vesicles. *Proc Natl Acad Sci USA* 111:E1140–E1148.
35. Carreras-Sureda A, Pihán P, Hetz C (2018) Calcium signaling at the endoplasmic reticulum: Fine-tuning stress responses. *Cell Calcium* 70:24–31.
36. Murphy E, et al. (2003) Coding potential of laboratory and clinical strains of human cytomegalovirus. *Proc Natl Acad Sci USA* 100:14976–14981.
37. Fiorio Pla A, et al. (2012) TRPV4 mediates tumor-derived endothelial cell migration via arachidonic acid-activated actin remodeling. *Oncogene* 31:200–212.